Eur. J. Mineral.
2018, **30**, 593–607
Published online 4 May 2018

Cryptochalcite, $K_2Cu_5O(SO_4)_5$, and cesiodymite, $CsKCu_5O(SO_4)_5$, two new isotypic minerals and the K–Cs isomorphism in this solid-solution series

IGOR V. PEKOV[1,*], NATALIA V. ZUBKOVA[1], ATALI A. AGAKHANOV[2], DMITRY Y. PUSHCHAROVSKY[1], VASILIY O. YAPASKURT[1], DMITRY I. BELAKOVSKIY[2], MARINA F. VIGASINA[1], EVGENY G. SIDOROV[3] and SERGEY N. BRITVIN[4]

[1] Faculty of Geology, Moscow State University, Vorobievy Gory, 119991 Moscow, Russia
*Corresponding author, e-mail: igorpekov@mail.ru
[2] Fersman Mineralogical Museum of Russian Academy of Sciences, Leninsky Prospekt 18-2, 119071 Moscow, Russia
[3] Institute of Volcanology and Seismology, Far Eastern Branch of Russian Academy of Sciences, Piip Boulevard 9, 683006 Petropavlovsk-Kamchatsky, Russia
[4] Department of Crystallography, St Petersburg State University, University Embankment 7/9, 199034 St Petersburg, Russia

Abstract: Two new isotypic minerals cryptochalcite, $K_2Cu_5O(SO_4)_5$, and cesiodymite, $CsKCu_5O(SO_4)_5$, were found in fumarole sublimates at the Second scoria cone of the Northern Breakthrough of the Great Tolbachik Fissure Eruption, Tolbachik volcano, Kamchatka, Russia. They are associated with one another and with euchlorine, chalcocyanite, alumoklyuchevskite, anglesite, fedotovite, wulffite, langbeinite, aphthitalite, steklite, hematite. Both minerals are visually indistinguishable from one another and form coarse tabular or prismatic crystals or grains up to 0.3 mm. They are brittle, transparent, light green to green, with vitreous lustre. Calculated densities for cryptochalcite and cesiodymite are 3.41 and 3.59 g cm^{-3}, respectively. Both are optically biaxial (–); cryptochalcite: α 1.610(3), β 1.632 (4), γ 1.643(4), $2V_{meas}$ 65(5)°; cesiodymite: α 1.61(1), β 1.627(4), γ 1.635(4), $2V_{meas}$ 70(10)°. The empirical formulae, based on 21 O *apfu*, are: cryptochalcite, $(K_{1.83}Na_{0.09}Rb_{0.09}Cs_{0.06})_{\Sigma 2.07}(Cu_{3.86}Zn_{1.02}Mg_{0.19})_{\Sigma 5.07}S_{4.97}O_{21}$; cesiodymite, $(K_{1.14}Rb_{0.16}Cs_{0.73})_{\Sigma 2.03}(Cu_{3.69}Zn_{1.33})_{\Sigma 5.02}S_{4.99}O_{21}$. Both minerals are triclinic, *P*-1, *Z* = 4; cryptochalcite: *a* 10.0045(3), *b* 12.6663(4), *c* 14.4397(5) Å, α 102.194 (3), β 101.372(3), γ 90.008(3)°, *V* 1751.7(1) Å^3; cesiodymite: *a* 10.0682(4), *b* 12.7860(7), *c* 14.5486(8) Å, α 102.038(5), β 100.847(4), γ 89.956(4)°, *V* 1797.5(2) Å^3. Their crystal structures are topologically identical and have been refined from single-crystal X-ray diffraction data to final agreement indices *R* = 0.0503 for cryptochalcite and 0.0898 for cesiodymite. They are based upon the heteropolyhedral $\{Cu_5O(SO_4)_5\}^{2-}$ framework composed by two types of alternating Cu^{2+}-S-O polyhedral layers $\{Cu_2(SO_4)_2\}^0$ and $\{Cu_3O(SO_4)\}^{2+}$ connected *via* SO_4 tetrahedra. K and Cs cations occupy sites in the tunnels of the framework. Cryptochalcite is named from Greek κρυπτός, concealed, and χαλκός, copper: it is associated with other green copper oxysulfates and is visually very similar to them. Cesiodymite is named from cesium and Greek δίδυμος, a twin brother, being a Cs-K-ordered analogue of cryptochalcite.

Key-words: cryptochalcite; cesiodymite; new mineral; alkali copper sulfate; oxysulfate; crystal structure; cesium potassium isomorphous substitution; fumarole; Tolbachik volcano; Kamchatka.

1. Introduction

Natural H-free alkali-copper oxysulfates (*i.e.*, sulfates with additional, non-bound with S^{6+} oxygen anion) form a distinctive family nowadays currently comprising fourteen minerals. They share common chemical features but differ strongly from each other in stoichiometry and nine structural types have been identified:

[1] a triad of isostructural (monoclinic, *C*2/*c*, *a* = 17.39–19.04, *b* = 9.40–9.48, *c* = 14.21–14.40 Å, β = 111.0–113.7°) euchlorine, $KNaCu_3O(SO_4)_3$ (Scordari & Stasi, 1990), fedotovite, $K_2Cu_3O(SO_4)_3$ (Vergasova *et al.*, 1988a; Starova *et al.*, 1991), and puninite, $Na_2Cu_3O(SO_4)_3$ (Siidra *et al.*, 2017) with the structures based on the $\{Cu_3O(SO_4)_3\}^{2-}$ heteropolyhedral layers;

[2,3] a pair of structurally related orthorhombic wulffite, $K_3NaCu_4O_2(SO_4)_4$ (*Pn*2$_1$*a*, *a* = 14.28, *b* = 4.95, *c* = 24.11 Å), and monoclinic parawulffite, $K_5Na_3Cu_8O_4(SO_4)_8$ (*P*2/*c*, *a* = 13.90, *b* = 4.98, *c* = 23.59 Å, β = 90.21°), with the heteropolyhedral chains $\{Cu_2O(SO_4)_2\}^{2-}$ (Pekov *et al.*, 2014a);

[4] orthorhombic kamchatkite, $KCu_3O(SO_4)_2Cl$ (*Pnma*, *a* = 9.76, *b* = 7.02, *c* = 12.89 Å, after Siidra *et al.*, 2017) (Vergasova *et al.*, 1988b; Varaksina *et al.*, 1990; Siidra *et al.*, 2017), with the $\{Cu_3O(SO_4)_2Cl\}^-$ heteropolyhedral framework;

https://doi.org/10.1127/ejm/2018/0030-2725
0935-1221/18/0030-2725 $6.75

Table 1. Comparative data of cryptochalcite and cesiodymite.

Mineral	Cryptochalcite		Cesiodymite	
Formula	$K_2Cu_5O(SO_4)_5$		$CsKCu_5O(SO_4)_5$	
Crystal system	Triclinic			
Space group	*P*-1			
Unit-cell parameters[*]	*SCXRD:*	*PXRD*:	*SCXRD*:	*PXRD*:
a, Å	10.0045(3)	10.00(3)	10.0682(4)	10.06(2)
b, Å	12.6663(4)	12.68(3)	12.7860(7)	12.79(2)
c, Å	14.4397(5)	14.435(3)	14.5486(8)	14.56(2)
α, °	102.194(3)	102.26(6)	102.038(5)	102.07(4)
β, °	101.372(3)	101.47(5)	100.847(4)	100.89(3)
γ, °	90.008(3)	89.87(5)	89.956(4)	89.94(4)
V, Å^3	1751.7(1)	1753(3)	1797.5(2)	1798(2)
Z	4	4	4	4
Strongest reflections of the powder X-ray diffraction pattern: *d*, Å–*I*	13.9–30 6.95–100 6.22–45 3.93–65 3.76–30 3.39–30 3.19–35 2.500–40		6.95–54 3.946–100 3.765–37 3.404–39 3.188–50 3.149–27 3.104–28 2.681–31	
Optical data:				
α	1.610(3)		1.61(1)	
β	1.632(4)		1.627(4)	
γ	1.643(4)		1.635(4)	
Optical sign, 2*V* (meas)	(–) 65°		(–) 70°	
Density (calc), g cm^{-3}	3.41		3.59	

[*] *SCXRD* and *PXRD* mean single-crystal and powder X-ray diffraction data, respectively.

[5] tetragonal (*I*4, *a* = 13.60, *c* = 4.98 Å, after Effenberger & Zemann, 1984) piypite, $K_8Cu_9O_4(SO_4)_8Cl_2$ (Effenberger & Zemann, 1984; Vergasova *et al.*, 1984), with heteropolyhedral chains $\{Cu_2O(SO_4)_2\}^{2-}$ topologically close to those found in wulffite and parawulffite;

[6] isomorphous series klyuchevskite, $K_3Cu_3Fe^{3+}O_2(SO_4)_4$ (monoclinic, *I*2, *a* = 18.77, *b* = 4.967, *c* = 18.468 Å, β = 101.66°) (Vergasova *et al.*, 1989; Gorskaya *et al.*, 1992) – alumoklyuchevskite, $K_3Cu_3AlO_2(SO_4)_4$ (triclinic, *P*-1, *a* = 4.95, *b* = 11.98, *c* = 14.63 Å, α = 87.12, β = 80.25, γ = 78.07°, after Siidra *et al.*, 2017) (Gorskaya *et al.*, 1995; Siidra *et al.*, 2017), or monoclinic (*I*2, *a* = 18.77, *b* = 4.97, *c* = 18.47 Å, β = 101.66°) (Krivovichev *et al.*, 2009) with the chains $\{[Cu_3O_2M(SO_4)_4\}^{3-}$ (*M* = Fe^{3+}, Al) as basic structural unit;

[7] isotypic tetragonal nabokoite, $KCu_7Te^{4+}O_4(SO_4)_5Cl$ (*P*4/*ncc*, *a* = 9.83, *c* = 20.59 Å: Pertlik & Zemann, 1988), with the complicated sheets $\{[Cu_7TeO_4(SO_4)_4SO_4]\}$ and atlasovite, $KCu_7Fe^{3+}Bi^{3+}O_4(SO_4)_5Cl$, which form a solid-solution series (Popova *et al.*, 1987);

[8] monoclinic eleomelanite, $(K_2Pb)Cu_4O_2(SO_4)_4$ (*P*2$_1$/*n*, *a* = 9.40, *b* = 4.89, *c* = 18.23 Å, β = 104.41°), with the heteropolyhedral chains $\{Cu_2O(SO_4)_2\}^{2-}$ topologically related to those in wulffite, parawulffite and piypite (Pekov *et al.*, 2016);

[9] isostructural triclinic (*P*-1) cryptochalcite, $K_2Cu_5O(SO_4)_5$, and cesiodymite, $CsKCu_5O(SO_4)_5$, (Table 1) containing the $\{Cu_5O(SO_4)_5\}^{2-}$ heteropolyhedral framework and first described in this paper.

All these minerals are endemic to oxidizing volcanic fumaroles. They condense directly from fumarolic gas at high temperatures, typically >350–400 °C, as shown by data reported in the above-cited papers and to our temperature measurements in fumarole chambers. All listed oxysulfates occur in active fumaroles of the Tolbachik volcano (Kamchatka, Russia), which is the type locality of thirteen of them, except for euchlorine first discovered at the Vesuvius volcano in Campania, Italy.

The name cryptochalcite (Cyrillic: криптохальцит) is derived from the Greek κρυπτός, concealed, and χαλκός, copper: this green copper mineral occurs in intimate association with other green copper oxysulfates and is visually very similar to them. This is especially the case for euchlorine and fedotovite which prevail in the type assemblage. In other words, the name cryptochalcite means "*concealed among other copper minerals*". The new mineral was initially distinguished from euchlorine and fedotovite based on a slight difference in colour:

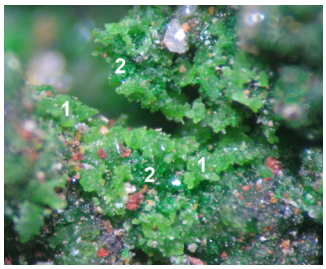

a

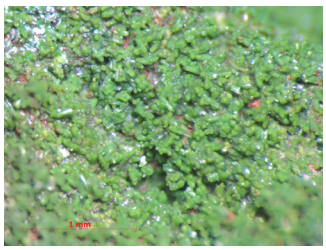

b

Fig. 1. Green aggregates of cryptochalcite (1) on a crust of deep green euchlorine (2) with colourless, transparent crystals of anglesite and iron-black hematite from the Arsenatnaya fumarole (a) and light green cryptochalcite crystal crust on basalt scoria from the Yadovitaya fumarole (b). Field of view: a – 2.7 mm, b – 2.8 mm. Photo: I.V. Pekov & A.V. Kasatkin.

cryptochalcite is somewhat lighter than the most common varieties of these oxysulfates (Fig. 1a). The name cesiodymite (цезиодимит) is derived from *cesi*um and Greek δίδυμοζ, a twin brother: the mineral contains species-defining cesium and is a Cs-K-ordered analogue of cryptochalcite.

Both new minerals and their names have been approved by the IMA Commission on New Minerals, Nomenclature and Classification (cryptochalcite, IMA No. 2014–106; cesiodymite, IMA No. 2016–002). The type specimens are deposited in the systematic collection of the Fersman Mineralogical Museum of the Russian Academy of Sciences, Moscow, with the catalogue numbers 95002 (cryptochalcite) and 95349 (cesiodymite).

2. Occurrence, general appearance and morphology

Both new minerals were detected in samples collected by us from active fumaroles located at the apical part of the Second scoria cone of the Northern Breakthrough of the Great Tolbachik Fissure Eruption (NB GTFE), Tolbachik volcano, Kamchatka Peninsula, Far-Eastern Region, Russia (55°41' N 160°14' E, 1200 m asl). Cryptochalcite is found in the Arsenatnaya (holotype) and Yadovitaya fumaroles whereas cesiodymite only in Arsenatnaya.

The Second scoria cone of the NB GTFE is a monogenetic volcano about 300 m high and approximately 0.1 km^3 in volume formed in 1975 (Fedotov & Markhinin, 1983) and demonstrating strong fumarolic activity to the present day. The general description of the Arsenatnaya fumarole is given by Pekov *et al.* (2014b, 2018) and of Yadovitaya by Vergasova & Filatov (2016).

In Arsenatnaya, areas enriched in alkali-copper sulfates mainly occur at the depths of 0.5–0.8 m from the surface. Cryptochalcite and cesiodymite belong to the same mineral assemblage and are associated with euchlorine, chalcocyanite, dolerophanite, alumoklyuchevskite, anglesite, fedotovite, wulffite, langbeinite, aphthitalite, piypite, klyuchevskite, eleomelanite, anhydrite, dravertite, krasheninnikovite, calciolangbeinite, steklite, hematite, tenorite, pseudobrookite, As-bearing orthoclase, sylvite, halite, lammerite, lammerite-β, urusovite, and gold (the associated minerals here and below are listed in order of their abundance, from common to rare species). The temperatures measured by us using a chromel-alumel thermocouple in these areas (inside cracks and chambers immediately after their uncovering) varied from 300 to 400 °C. Only H-free minerals occur in this hot zone. They deposited directly from volcanic gas (an obvious source of S, Cu and alkali metals) as sublimates or formed as the result of interaction between gas and host basalt. Above this hot zone, in the outer zone of the fumarole in which the sublimate sulfates and chlorides react with atmospheric water and water vapour, kaliochalcite, gypsum, chalcantite, bonattite, and eriochalcite form as secondary minerals.

Cryptochalcite in Arsenatnaya occurs as poorly-formed prismatic crystals or grains irregular in shape up to 0.1 mm × 0.1 mm × 0.3 mm in size and their open-work aggregates (Fig. 1a) up to 1.2 mm across. Cesiodymite forms crude prismatic or thick tabular crystals (Fig. 2) up to 0.05 mm × 0.1 mm × 0.15 mm or grains (up to 0.3 mm in size) and their clusters, crusts or open-work aggregates up to 0.5 mm across. Both new minerals overgrow encrustations of other sulfates: typically euchlorine, sometimes anglesite, chalcocyanite, dolerophanite, alumoklyuchevskite or aphthitalite (Figs. 1–4), that cover basalt scoria altered by fumarolic gases.

In the Yadovitaya fumarole cryptochalcite was found as crude, roundish, usually blocky, prismatic crystals up to 0.08 mm × 0.2 mm forming discontinuous crusts (Fig. 1b) up to 1.5 cm × 2 cm in area and up to 0.2 mm thick

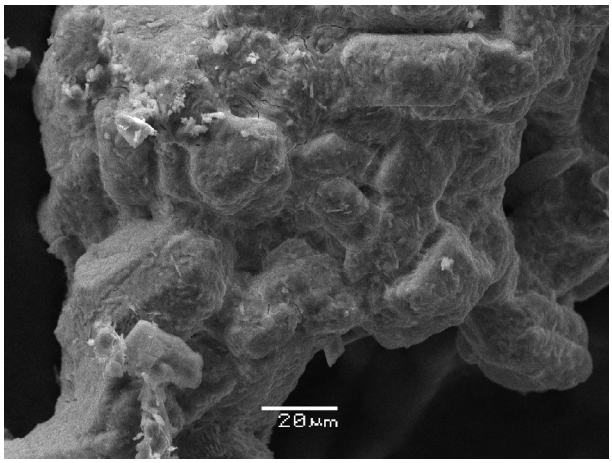

Fig. 2. Cluster of crude crystals of cesiodymite. Scanning electron microscope (SEM) image (secondary electrons).

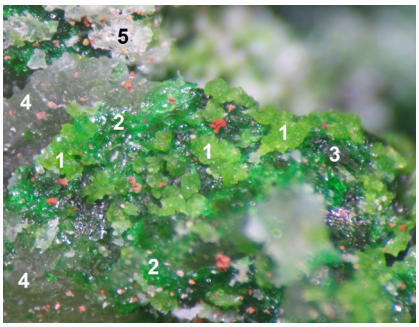

Fig. 4. Close association of five high-temperature sulfates in sublimate incrustations of the Arsenatnaya fumarole: 1–cesiodymite, $CsKCu_5O(SO_4)_5$, 2–euchlorine, $KNaCu_3O(SO_4)_3$, 3–alumoklyuchevskite, $K_3Cu_3(Al,Fe^{3+})O_2(SO_4)_4$, 4–chalcocyanite, $CuSO_4$, and 5–aphthitalite, $K_3Na(SO_4)_2$. Field of view: 2.7 mm. Photo: I.V. Pekov & A.V. Kasatkin.

covering basalt scoria. Closely associated minerals are euchlorine, alumoklyuchevskite, langbeinite, steklite, fedotovite, hematite, and lyonsite. The temperature measured in the area where cryptochalcite occurs was *ca.* 300 °C.

Both minerals are triclinic (space group *P*-1) and their crystals are formed by pinacoidal faces only. The crude character of crystals prevented the indexing of forms.

3. Physical properties and optical data

Cryptochalcite and cesiodymite are visually indistinguishable from one another. Both minerals are transparent (in aggregates sometimes translucent) light green to green, sometimes with a yellow hue. The streak is pale green. The lustre is vitreous. The minerals are brittle. Cleavage or parting was not observed, the fracture is uneven. The Mohs' hardness is *ca.* 3. Density could not be measured because of the small size of individual crystals and the porous character of aggregates. The density values calculated from empirical formulae for the holotype specimens of cryptochalcite and cesiodymite are 3.411 and 3.593 g cm^{-3}, respectively.

Both new minerals are optically biaxial (–), no dispersion of the optical axes was observed. Refractive indices and $2V$ values (589 nm) of the holotypes are: $\alpha = 1.610(3)$, $\beta = 1.632(4)$, $\gamma = 1.643(4)$, $2V_{meas} = 65(5)°$, and $2V_{calc} = 70°$ for cryptochalcite and $\alpha = 1.61(1)$, $\beta = 1.627(4)$, $\gamma = 1.635(4)$, $2V_{meas} = 70(10)°$, and $2V_{calc} = 68°$ for cesiodymite. Both minerals show distinct pleochroism with the following absorption schemes: cryptochalcite, Z (bright green) $> Y$ (green, with a weak yellow hue) $> X$ (pale green to almost colourless); cesiodymite, $Z \approx Y$ (lettuce green) $> X$ (pale green to almost colourless).

4. Raman spectroscopy

The Raman spectra of cryptochalcite and cesiodymite (Fig. 5) were obtained using an EnSpectr R532 spectrophotometer with a green laser (532 nm) under the same conditions, at room temperature. The output power of the laser beam was about 3.5 mW. The spectra were processed using the EnSpectr expert mode program in the range 100 to 4000 cm^{-1} with the use of a holographic diffraction grating with 1800 mm^{-1} and a resolution equal to 6 cm^{-1}. The diameter of the focal spot on each sample was about 10 µm. The spectra were obtained for randomly oriented crystals.

Bands in the Raman spectra of new minerals are observed in the following regions (cm^{-1}; assignments according to Nakamoto, 1986): 1200–1050 [$F_2(\nu_3)$-type stretching vibrations of SO_4^{2-}], 1030–950 [$A_1(\nu_1)$ symmetric stretching vibrations of SO_4^{2-}], 670–590

[$F_2(\nu_4)$ bending vibrations of SO_4^{2-}], 500–420 [$E(\nu_2)$ bending vibrations of SO_4^{2-}], and 320–100 (lattice modes). The Raman spectra of cryptochalcite and cesiodymite are similar in general pattern but demonstrate some difference in wavenumbers and intensities of bands (Fig. 5).

The absence of bands with frequencies higher than 1200 cm^{-1} indicates the absence of groups with O–H, C–H, C–O, N–H and N–O bonds in both new minerals.

5. Chemical data

Chemical data for cryptochalcite and cesiodymite were obtained in two laboratories using: (1) a Jeol JSM-6480LV scanning electron microscope equipped with an INCA-Wave 500 wavelength-dispersive spectrometer (Laboratory of Analytical Techniques of High Spatial Resolution, Dept. of Petrology, Moscow State University), with an accelerating voltage of 20 kV, a beam current of 20 nA, and a 3 μm beam diameter; (2) a Jeol 733 electron microprobe instrument (Fersman Mineralogical Museum of Russian Academy of Sciences) operated in energy-dispersive mode with an accelerating voltage of 20 kV, a beam current of 2 nA, and a beam diameter of 5 μm. The latter was used to control the correctness of determination of alkali cations, avoiding damage of samples under high beam current. The same standards were used in both laboratories, except of one for Cu: albite (Na), microcline (K), $Rb_2Nb_4O_{11}$ (Rb), $Cs_2Nb_4O_{11}$ (Cs), diopside (Mg), and ZnS (Zn and S); $CuFeS_2$ and Cu were used for Cu in (1) and (2), respectively. Contents of other elements with atomic numbers higher than oxygen are below their detection limits. Special attention was paid for checking of Na, to avoid possible overlap of Na*K*α and Zn*L*α analytical lines.

Representative chemical data for cryptochalcite and cesiodymite are given in Table 2. Both minerals have the same stoichiometry corresponding to the idealized formula $A^+_2M^{2+}_5O(SO_4)_5$ in which A = **K**, **Cs**, Rb, Na and M = **Cu**, Zn, Mg (species-defining cations in bold type). The idealized formulae of cryptochalcite and cesiodymite are $K_2Cu_5O(SO_4)_5$ and $CsKCu_5O(SO_4)_5$, respectively. The chemical composition of the new minerals demonstrates significant variations in ratios of both A and M cations. Samples from Arsenatnaya are enriched in Zn while in cryptochalcite from Yadovitaya Mg>Zn. The Cs:K ratio varies in a wide range (Table 2, Fig. 6) – see Discussion.

Cryptochalcite and cesiodymite readily hydrolyse (become dull and bluish for several minutes) and slowly dissolve in H_2O at room temperature.

6. X-ray crystallography

Powder X-ray diffraction (XRD) data of cryptochalcite (Table 3, deposited, *i.e.* freely available as Supplementary Material linked to this article on the GSW website of the journal: https://pubs.geoscienceworld.org/eurjmin/) and cesiodymite (Table 4, deposited) were collected with a 114.6 mm diameter Debye-Scherrer camera (Fe*K*α radiation) and with a Rigaku R-AXIS Rapid II single-crystal diffractometer equipped with a cylindrical image plate detector (Debye-Scherrer geometry; d = 127.4 mm; Co*K*α radiation), respectively. The unit-cell parameters refined from these powder data are reported in Table 1. The powder XRD patterns and unit-cell dimensions of cryptochalcite and cesiodymite are very similar.

Single-crystal XRD studies of both minerals were carried out for the holotypes using a four-circle Xcalibur S diffractometer equipped with a CCD detector. A complete sphere of three-dimensional data was collected for each mineral. Intensity data were corrected for Lorentz and polarization effects. Crystal structures of cryptochalcite and cesiodymite were solved by direct methods and refined to R = 0.0503 and 0.0898, respectively, using the SHELX software package (Sheldrick, 2015). For both minerals the crystal data, data collection information and structure refinement details are summarized in Table 5, atom coordinates and displacement parameters, site occupancies and bond valence sums are given in Table 6 and selected interatomic distances in Table 7.

Table 2. Chemical composition of cryptochalcite and cesiodymite.

	1	2	3*	4	5	6	7*	8	9	10	11	12	13
wt%													
Na_2O	–	1.02	0.30 (0.22–0.38)	0.15	–	–	–	–	–	–	–	–	
K_2O	10.56	9.30	9.55 (9.27–9.84)	9.20	8.45	5.77	5.47 (4.78–5.77)	4.85	4.45	4.23	4.09	3.21	4.78
Rb_2O	–	0.20	0.89 (0.80–1.02)	1.02	1.53	1.41	1.55 (1.39–1.67)	1.47	1.26	1.50	1.40	1.95	
Cs_2O	–	–	0.90 (0.72–1.08)	1.55	3.01	10.39	10.48 (9.98–11.13)	12.15	12.65	12.60	13.46	14.71	14.29
MgO	–	2.13	0.83 (0.68–1.05)	0.71	0.88	–	–	0.19	–	0.24	0.57	0.44	
CuO	44.58	39.47	33.95 (32.95–34.80)	35.86	35.92	30.23	29.91 (29.08–30.62)	29.53	29.50	29.91	27.86	27.29	40.34
ZnO	–	1.36	9.14 (8.83–9.48)	7.71	6.48	11.33	11.05 (10.45–11.67)	11.37	11.09	10.35	11.54	12.30	
SO_3	44.86	45.66	44.06 (43.17–44.60)	44.89	43.98	41.35	40.74 (39.71–41.17)	41.45	40.71	40.11	41.21	40.96	40.59
Total	100	99.14	99.62	101.09	100.25	100.48	99.20	101.01	99.66	98.94	100.13	100.86	100
Formula calculated on the basis of 21 O *apfu*													
Na	–	0.29	0.09	0.04	–	–	–	–	–	–	–	–	–
K	2	1.73	1.83	1.74	1.63	1.18	1.14	1.00	0.93	0.89	0.85	0.67	1
Rb	–	0.02	0.09	0.10	0.15	0.15	0.16	0.15	0.13	0.16	0.15	0.21	
Cs	–	–	0.06	0.10	0.19	0.71	0.73	0.83	0.88	0.89	0.93	1.03	1
Mg	–	0.46	0.19	0.16	0.20	–	–	0.05	–	0.06	0.14	0.11	–
Cu	5	4.35	3.86	4.02	4.11	3.67	3.69	3.59	3.65	3.74	3.42	3.37	5
Zn	–	0.15	1.02	0.84	0.72	1.34	1.33	1.35	1.34	1.27	1.39	1.49	–
S	5	5.01	4.97	5.00	4.99	4.99	4.99	5.01	5.01	4.99	5.03	5.03	5
ΣA^{+}**	2	2.04	2.07	1.98	1.97	2.04	2.03	1.98	1.94	1.94	1.93	1.91	2
ΣM^{2+}***	5	4.96	5.07	5.02	5.03	5.01	5.02	5.01	4.99	5.07	4.95	4.97	5

1 – $K_2Cu_5O(SO_4)_5$, 2 to 5 – cryptochalcite, 6 to 12 – cesiodymite, 13 – $CsKCu_5O(SO_4)_5$; 2 – Yadovitaya fumarole, 3 to 12 – Arsenatnaya fumarole.

* The holotype samples (3 – average for 4 analyses, 7 – average for 5 analyses, ranges are in parentheses).

** A^+ = Na, K, Rb, Cs.

*** M^{2+} = Mg, Cu, Zn. Dash means a constituent content below detection limit. Analyses 2–12 are ordered by increasing Cs:K ratio.

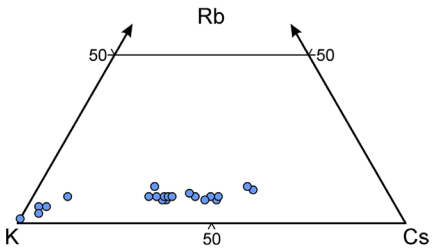

Fig. 6. Ratios of K, Rb and Cs in cryptochalcite and cesiodymite.

7. Discussion

7.1. Crystal structure

Cryptochalcite and cesiodymite are isostructural. They differ from one another, in fact, only in the ratio and distribution of K and Cs between the *A* sites and in the coordination of *A* cations. The minerals share a novel structure type. Below we describe both crystal structures together, as a cryptochalcite/cesiodymite structure, and use the same term in the captions to Figs. 7–10.

The crystal structure of these minerals (Fig. 7) is based upon the heteropolyhedral framework $\{Cu_5O(SO_4)_5\}^{2-}$ composed of two types of alternating Cu^{2+}–S–O polyhedral layers $\{Cu_2(SO_4)_2\}^0$ and $\{Cu_3O(SO_4)\}^{2+}$ coplanar to the *ab* plane and connected *via* SO_4 tetrahedra. No evidence of Cu–Zn or Cu–Mg ordering was found in the new minerals, and we mark all *M* sites as Cu due to its dominance at these sites (Tables 6–7, Figs. 7–9). *Layer I* (Fig. 8a) consists of clusters formed by four edge-sharing octahedra with significant Janh-Teller distortion. There are two symmetrically independent clusters in *layer I*: one is formed by two Cu(4)- and two Cu(6)-centred octahedra, and the second one by two Cu(3)- and two Cu(5)-centred octahedra. The distortion of the octahedra is different: Cu (5)- and Cu(6)-centred octahedra are characterized by a [4 + 2] distortion with four short Cu–O distances and two elongated bonds close to each other, while Cu(3)- and Cu (4)-centred octahedra have a [4 + 1 + 1] coordination with four short Cu–O distances one elongated bond and one strongly elongated Cu–O bond (Table 7). These kinds of distortion are typical of Cu-centred polyhedra in general; the geometry of mixed-ligand $Cu^{2+}\Phi_6$ octahedra ($\Phi = O^{2-}$, OH^-, H_2O^0 and Cl^-) was examined by Burns & Hawthorne (1995). The clusters are connected with each other by Cu(1)- and Cu(2)-centred tetragonal pyramids sharing common vertices with the octahedra of adjacent clusters. The linkage between Cu-centred polyhedra in *layer I* is reinforced by $S(3)O_4$ and $S(4)O_4$ tetrahedra. *Layer II* (Fig. 8b) is formed by isolated from each other Cu (7)- and Cu(9)-centred tetragonal pyramids alternating with Cu(8)- and Cu(10)-centred trigonal bipyramids (Table 7). These polyhedra are connected *via* $S(1)O_4$, S (2)O_4, $S(9)O_4$ and $S(10)O_4$ tetrahedra sharing common vertices. Adjacent *layers I* and *II* are connected *via* S(5–8)-centred tetrahedra (Fig. 7).

Table 5. Crystal data, data collection information and structure refinement details for cryptochalcite and cesiodymite.

Mineral	Cryptochalcite	Cesiodymite
Formula weight	900.12*	967.40
Temperature, K	293(2)	
Radiation and wavelength, Å	Mo$K\alpha$; 0.71073	
Crystal system, space group, Z	Triclinic, P-1; 4	
Unit-cell dimensions, Å,°	a = 10.0045(3) α = 102.194(3) b = 12.6663(4) β = 101.372(3) c = 14.4397(5) γ = 90.008(3)	a = 10.0682(4) α = 102.038(5) b = 12.7860(7) β = 100.847(4) c = 14.5486(8) γ = 89.956(4)
V, Å^3	1751.73(10)	1797.52(16)
Absorption coefficient μ, mm^{-1}	7.205*	8.643
F_{000}	1739*	1840
Crystal size, mm	0.05 × 0.10 × 0.17	0.03 × 0.05 × 0.05
Diffractometer	Xcalibur S CCD	
θ range for data collection,°	2.59–28.28	2.68–28.28
Index ranges	$-13 \le h \le 13$, $-16 \le k \le 16$, $-19 \le l \le 19$	$-13 \le h \le 12$, $-17 \le k \le 16$, $-19 \le l \le 19$
Reflections collected	30618	25734
Independent reflections	8706 (R_{int} = 0.0554)	8458 (R_{int} = 0.0934)
Independent reflections with $I > 2\sigma(I)$	6715	4302
Data reduction	CrysAlisPro, Agilent Technologies, v. 1.171.37.34 (Agilent Technologies, 2014)	
Absorption correction	Analytical [Analytical numeric absorption correction using a multifaceted crystal model based on expressions derived by Clark & Reid (1995)]	
Structure solution	Direct methods	
Refinement method	Full-matrix least-squares on F^2	
Number of refined parameters	599	597
Final R indices [$I > 2\sigma(I)$]	$R1$ = 0.0503, w$R2$ = 0.0917	$R1$ = 0.0898, w$R2$ = 0.1823
R indices (all data)	$R1$ = 0.0739, w$R2$ = 0.0991	$R1$ = 0.1747, w$R2$ = 0.2264
GoF	1.098	1.032
Largest diff. peak and hole, e/Å^3	1.46 and −0.88	4.02 and −1.97

* Calculated on the basis of e_{ref} for K(1), K(2), K(3) and K(4) positions.

Table 6. Coordinates, equivalent displacement parameters (U_{eq}, in Å^2) of atoms, site occupancy factors (s.o.f.) and bond valence sums (BVS) for cryptochalcite (first line of each row) and cesiodymite (second line of each row).

Site	x	y	z	U_{eq}	s.o.f.*	BVS**
A(1)	0.41785(13)	0.71943(13)	0.73397(10)	0.0390(5)	K	0.74
	0.42820(16)	0.42820(16)	0.73518(11)	0.0356(7)	$Cs_{0.531(6)}K_{0.469(6)}$	1.03
A(2)	0.57672(14)	0.86012(14)	0.26886(11)	0.0353(5)	K	0.92
	0.5770(2)	0.8439(3)	0.26538(17)	0.0569(9)	$K_{0.63}Cs_{0.21}Rb_{0.16}$*	1.09
A(3)	0.08161(14)	0.34368(14)	0.26283(11)	0.0395(6)	K	0.76
	0.07497(18)	0.33061(17)	0.26166(13)	0.0383(8)	$K_{0.583(6)}Cs_{0.417(6)}$	1.01
A(4)	0.07806(13)	0.76734(12)	0.27414(10)	0.0326(5)	K	0.92
	0.07402(19)	0.78245(19)	0.26999(14)	0.0431(6)	$K_{0.55}Cs_{0.29}Rb_{0.16}$*	1.01
Cu(1)	0.70596(6)	0.09487(5)	−0.00830(5)	0.01054(15)	1	2.07
	0.71210(19)	0.09831(14)	−0.00716(13)	0.0204(5)		2.05
Cu(2)	0.79459(6)	0.59929(5)	0.00826(5)	0.01053(15)	1	2.09
	0.78809(19)	0.60145(14)	0.00663(13)	0.0213(5)		2.04
Cu(3)	0.76308(7)	0.87643(5)	−0.00308(5)	0.01103(15)	1	1.98
	0.7596(2)	0.87975(14)	−0.00229(13)	0.0198(4)		1.91
Cu(4)	0.73685(6)	0.37871(5)	0.00319(5)	0.01083(15)	1	1.99
	0.7398(2)	0.38122(14)	0.00297(13)	0.0200(4)		1.92
Cu(5)	0.97292(6)	0.97291(5)	0.89612(5)	0.01014(15)	1	2.00
	0.97478(16)	0.97430(13)	0.89755(12)	0.0128(4)		2.01
Cu(6)	0.47333(6)	0.47771(5)	0.89609(5)	0.01037(15)	1	2.04
	0.47479(16)	0.47689(13)	0.89745(12)	0.0137(4)		2.03
Cu(7)	0.16268(6)	0.89806(5)	0.59074(5)	0.01188(15)	1	2.09
	0.16576(17)	0.89776(13)	0.58912(12)	0.0139(4)		2.02
Cu(8)	0.33084(6)	0.10038(5)	0.41059(5)	0.01130(15)	1	1.93
	0.33407(17)	0.10030(13)	0.41253(12)	0.0114(4)		1.89
Cu(9)	0.33799(6)	0.60493(6)	0.41023(5)	0.01206(15)	1	2.07
	0.33425(17)	0.60408(13)	0.41055(12)	0.0140(4)		2.02
Cu(10)	0.16856(6)	0.40351(5)	0.58825(5)	0.01141(15)	1	1.89
	0.16576(16)	0.40179(13)	0.58766(12)	0.0108(4)		1.87

Table 6. (continued).

Site	*x*	*y*	*z*	U_{eq}	s.o.f.*	BVS**
S(1)	0.61274(13)	0.13989(11)	0.55449(10)	0.0106(3)	1	6.06
	0.6114(3)	0.1426(3)	0.5523(3)	0.0125(8)		6.08
S(2)	0.61730(13)	0.63517(11)	0.54464(10)	0.0108(3)	1	6.09
	0.6168(3)	0.6338(3)	0.5422(2)	0.0123(8)		6.08
S(3)	0.97506(13)	0.24171(11)	−0.01071(11)	0.0122(3)	1	6.04
	0.9799(4)	0.2427(3)	−0.0079(3)	0.0264(10)		6.13
S(4)	0.47689(13)	0.25400(11)	−0.00902(11)	0.0125(3)	1	6.06
	0.4798(4)	0.2546(3)	−0.0082(3)	0.0245(10)		6.21
S(5)	0.32366(12)	0.05543(11)	0.19953(10)	0.0111(3)	1	6.07
	0.3179(3)	0.0516(3)	0.1978(2)	0.0128(8)		6.00
S(6)	0.22211(12)	−0.04344(11)	0.81199(10)	0.0099(3)	1	6.08
	0.2224(3)	−0.0443(3)	0.8121(2)	0.0120(7)		6.01
S(7)	0.27762(12)	0.54529(11)	0.18835(10)	0.0095(3)	1	6.08
	0.2776(3)	0.5447(3)	0.1875(2)	0.0115(7)		6.03
S(8)	0.17660(13)	0.45684(11)	0.80021(10)	0.0108(3)	1	6.03
	0.1819(3)	0.4561(3)	0.8027(2)	0.0136(8)		6.08
S(9)	0.11588(13)	0.13719(11)	0.54474(10)	0.0106(3)	1	6.10
	0.1169(3)	0.1348(3)	0.5435(2)	0.0111(7)		6.11
S(10)	0.88585(13)	0.35675(11)	0.44620(10)	0.0108(3)	1	6.13
	0.8866(3)	0.3556(3)	0.4483(2)	0.0120(8)		6.17
O(1)	0.2754(3)	0.9366(3)	0.7222(3)	0.0120(8)	1	2.15
	0.2750(9)	0.9344(7)	0.7233(6)	0.016(2)		2.11
O(2)	0.0169(4)	0.8348(3)	0.0995(3)	0.0231(10)	1	1.95
	0.0168(14)	0.8348(8)	0.0953(10)	0.052(4)		2.08
O(3)	0.8163(4)	0.9355(3)	0.7846(3)	0.0177(9)	1	1.97
	0.8217(9)	0.9411(8)	0.7864(7)	0.020(2)		2.00
O(4)	0.1712(4)	0.0585(3)	0.6027(3)	0.0227(10)	1	2.06
	0.1728(11)	0.0569(8)	0.5993(7)	0.026(3)		2.09
O(5)	0.3640(3)	0.4942(3)	−0.0026(3)	0.0090(8)	1	1.91
	0.3644(8)	0.4956(6)	−0.0028(6)	0.0091(19)		1.93
O(6)	0.7401(4)	0.9318(3)	0.1355(3)	0.0171(9)	1	2.00
	0.7347(11)	0.9344(8)	0.1341(7)	0.026(3)		1.97
O(7)	0.8526(4)	0.4385(3)	0.1424(3)	0.0207(9)	1	1.93
	0.8462(10)	0.4393(8)	0.1414(7)	0.026(3)		1.96
O(8)	0.0340(4)	0.8663(3)	0.4676(3)	0.0184(9)	1	2.11
	0.0322(9)	0.8701(8)	0.4688(6)	0.017(2)		2.07
O(9)	0.1491(4)	0.7518(3)	0.6173(3)	0.0197(9)	1	2.04
	0.1432(10)	0.7521(7)	0.6147(7)	0.020(2)		2.05
O(10)	0.2136(4)	0.4412(3)	0.1311(3)	0.0224(10)	1	2.09
	0.2179(11)	0.4397(8)	0.1318(7)	0.029(3)		2.05
O(11)	0.0736(4)	0.9389(3)	0.7892(3)	0.0191(9)	1	1.98
	0.0749(9)	0.9430(8)	0.7911(7)	0.020(2)		2.02
O(12)	0.3448(4)	0.9442(3)	0.1500(3)	0.0213(9)	1	2.07
	0.3406(10)	0.9411(8)	0.1472(7)	0.025(3)		2.00
O(13)	0.3304(3)	0.2563(3)	0.0025(3)	0.0129(8)	1	2.10
	0.3316(10)	0.2546(8)	0.0022(7)	0.026(3)		2.01
O(14)	0.4866(4)	0.2892(3)	0.9028(3)	0.0240(10)	1	1.96
	0.4843(15)	0.2884(9)	0.9043(10)	0.055(4)		2.16
O(15)	0.3492(4)	0.8709(4)	0.5385(3)	0.0221(10)	1	1.90
	0.3479(9)	0.8653(8)	0.5388(7)	0.022(2)		1.94
O(16)	0.9390(4)	0.7902(3)	0.9274(3)	0.0216(10)	1	1.93
	0.9420(12)	0.7908(9)	0.9257(10)	0.059(4)		2.09
O(17)	0.4383(4)	0.6746(3)	0.9254(3)	0.0235(10)	1	1.96
	0.4431(13)	0.6748(9)	0.9269(10)	0.064(5)		2.17
O(18)	0.3174(4)	0.4580(3)	0.7847(3)	0.0174(9)	1	1.96
	0.3211(10)	0.4557(8)	0.7867(7)	0.024(2)		2.02
O(19)	0.4838(4)	0.8577(3)	0.0142(3)	0.0155(9)	1	2.00
	0.4815(10)	0.8564(8)	0.0111(8)	0.030(3)		1.94
O(20)	0.8300(3)	0.2458(3)	0.0027(3)	0.0117(8)	1	2.13
	0.8321(11)	0.2459(8)	0.0032(8)	0.025(3)		2.00
O(21)	0.8438(4)	0.6306(3)	0.1500(3)	0.0206(10)	1	2.06
	0.8411(11)	0.6301(8)	0.1470(7)	0.028(3)		2.03
O(22)	0.3531(4)	0.1324(3)	0.1424(3)	0.0200(9)	1	1.94
	0.3491(10)	0.1287(8)	0.1414(7)	0.023(2)		1.95
O(23)	0.0164(3)	0.3514(3)	−0.0154(3)	0.0163(9)	1	1.98

Table 6. (continued).

Site	x	y	z	U_{eq}	s.o.f.*	BVS**
	0.0192(11)	0.3510(8)	−0.0109(8)	0.037(3)		1.99
O(24)	0.5733(4)	0.4621(4)	0.7892(3)	0.0197(10)	1	1.97
	0.5741(9)	0.4605(9)	0.7911(7)	0.026(3)		1.99
O(25)	0.7154(4)	0.1211(3)	0.1310(3)	0.0208(10)	1	2.07
	0.7182(11)	0.1233(8)	0.1310(7)	0.028(3)		2.00
O(26)	0.7590(4)	0.3679(3)	0.8640(3)	0.0181(9)	1	1.98
	0.7638(10)	0.3706(7)	0.8659(7)	0.020(2)		1.96
O(27)	0.8636(3)	0.0035(3)	−0.0024(3)	0.0081(7)	1	1.92
	0.8642(9)	0.0047(7)	−0.0014(6)	0.015(2)		1.92
O(28)	0.6698(4)	0.5545(3)	0.6012(3)	0.0203(10)	1	2.04
	0.6739(10)	0.5543(7)	0.5993(7)	0.023(3)		1.96
O(29)	0.1494(4)	0.6358(4)	0.4604(3)	0.0200(9)	1	1.92
	0.1519(9)	0.6392(7)	0.4598(6)	0.017(2)		1.94
O(30)	0.6800(4)	0.7391(3)	0.6019(3)	0.0205(9)	1	1.95
	0.6739(10)	0.7381(7)	0.5989(7)	0.021(2)		1.95
O(31)	0.6487(4)	0.6105(3)	0.4483(3)	0.0189(9)	1	1.99
	0.6524(10)	0.6117(8)	0.4474(7)	0.026(3)		1.99
O(32)	0.0336(4)	0.3783(3)	0.4585(3)	0.0176(9)	1	2.00
	0.0335(9)	0.3777(8)	0.4639(7)	0.022(2)		2.09
O(33)	0.7747(3)	0.4314(3)	0.7218(3)	0.0132(8)	1	2.17
	0.7734(8)	0.4329(7)	0.7230(6)	0.0094(19)		2.11
O(34)	0.5364(3)	0.8772(3)	0.4594(3)	0.0167(9)	1	2.02
	0.5367(9)	0.8787(8)	0.4638(7)	0.023(3)		2.06
O(35)	0.5822(3)	0.9194(3)	0.7058(3)	0.0154(9)	1	2.03
	0.5895(9)	0.9246(8)	0.7090(7)	0.023(2)		2.04
O(36)	0.6828(4)	0.0640(3)	0.6111(3)	0.0212(10)	1	1.95
	0.6781(11)	0.0670(8)	0.6071(7)	0.026(3)		1.99
O(37)	0.0822(4)	0.4347(3)	0.7053(3)	0.0167(9)	1	2.02
	0.0900(9)	0.4342(8)	0.7097(7)	0.021(2)		2.05
O(38)	0.6515(4)	0.2487(3)	0.6167(3)	0.0207(10)	1	2.04
	0.6453(10)	0.2504(7)	0.6162(7)	0.021(2)		2.00
O(39)	0.5328(4)	0.3629(3)	0.4661(3)	0.0185(9)	1	2.06
	0.5302(10)	0.3693(8)	0.4689(7)	0.022(2)		2.16
O(40)	0.1489(4)	0.1123(4)	0.4485(3)	0.0206(10)	1	1.97
	0.1530(10)	0.1113(8)	0.4487(7)	0.029(3)		1.98
O(41)	0.1898(4)	0.5681(3)	0.6071(3)	0.0217(10)	1	1.99
	0.1842(10)	0.5691(8)	0.6042(7)	0.027(3)		2.03
O(42)	0.1727(4)	0.2428(3)	0.6014(3)	0.0214(10)	1	1.96
	0.1707(10)	0.2400(7)	0.6000(7)	0.023(2)		1.95

* For the A(1–4) sites in cryptochalcite e_{ref} values calculated using K scattering curve are: A(1) 21.83, A(2) 20.25, A(3) 21.09 and A(4) 20.54.
** For the A(1–4) sites in cryptochalcite the bond valences were calculated for pure K sites. Thus, the sums could be slightly increased taking into account the admixtures of Cs and Rb, especially for the A(1) and A(3) sites characterized by the highest values of e_{ref}. Bond-valence parameters were taken from Brese & O'Keeffe (1991).

Table 7. Selected interatomic distances (Å) in the structures of cryptochalcite and cesiodymite.

Cryptochalcite*				Cesiodymite**			
A(1)–O(17)	2.906(5)	A(3)–O(16)	2.876(5)	A(1)–O(17)	2.887(15)	A(3)–O(16)	2.816(15)
A(1)–O(9)	2.956(4)	A(3)–O(32)	2.901(4)	A(1)–O(39)	3.035(10)	A(3)–O(32)	2.986(10)
A(1)–O(22)	2.989(4)	A(3)–O(28)	2.952(4)	A(1)–O(22)	3.086(9)	A(3)–O(28)	3.081(10)
A(1)–O(39)	2.994(4)	A(3)–O(10)	2.979(4)	A(1)–O(41)	3.110(10)	A(3)–O(10)	3.117(10)
A(1)–O(25)	3.003(4)	A(3)–O(7)	3.005(4)	A(1)–O(25)	3.149(10)	A(3)–O(7)	3.129(11)
A(1)–O(41)	3.017(4)	A(3)–O(30)	3.104(4)	A(1)–O(9)	3.183(10)	A(3)–O(30)	3.177(10)
A(1)–O(1)	3.120(4)	A(3)–O(33)	3.137(4)	A(1)–O(1)	3.295(10)	A(3)–O(33)	3.335(9)
A(1)–O(35)	3.159(4)	A(3)–O(37)	3.246(4)	A(1)–O(35)	3.331(10)	A(3)–O(9)	3.386(10)
		A(3)–O(9)	3.499(4)	A(1)–O(30)	3.515(10)	A(3)–O(37)	3.422(11)
				A(1)–O(18)	3.672(10)	A(3)–O(3)	3.592(10)
				A(1)–O(24)	3.673(11)	A(3)–O(41)	3.624(11)
						A(3)–O(11)	3.682(9)
A(2)–O(14)	2.743(5)			A(2)–O(14)	2.650(14)		
A(2)–O(34)	2.822(4)	A(4)–O(2)	2.787(4)	A(2)–O(34)	2.932(10)	A(4)–O(2)	2.719(14)
A(2)–O(4)	2.866(4)	A(4)–O(38)	2.881(4)	A(2)–O(4)	2.988(10)	A(4)–O(8)	2.984(9)

Table 7. (continued).

Cryptochalcite*				Cesiodymite**			
A(2)–O(1)	2.935(4)	*A*(4)–O(33)	2.922(4)	*A*(2)–O(12)	3.083(11)	*A*(4)–O(38)	3.071(11)
A(2)–O(12)	2.943(4)	*A*(4)–O(8)	2.928(4)	*A*(2)–O(6)	3.095(10)	*A*(4)–O(21)	3.078(9)
A(2)–O(6)	3.030(4)	*A*(4)–O(21)	2.955(4)	*A*(2)–O(1)	3.162(9)	*A*(4)–O(26)	3.162(9)
A(2)–O(35)	3.203(4)	*A*(4)–O(26)	3.068(4)	*A*(2)–O(42)	3.232(11)	*A*(4)–O(33)	3.163(9)
A(2)–O(42)	3.267(4)	*A*(4)–O(37)	3.117(4)	*A*(2)–O(35)	3.387(11)	*A*(4)–O(36)	3.166(9)
A(2)–O(36)	3.426(5)	*A*(4)–O(36)	3.158(4)	*A*(2)–O(38)	3.428(10)	*A*(4)–O(37)	3.319(9)
		A(4)–O(42)	3.378(5)	*A*(2)–O(36)	3.499(11)	*A*(4)–O(42)	3.423(10)
		A(4)–O(29)	3.414(4)	*A*(2)–O(19)	3.680(12)	*A*(4)–O(29)	3.591(10)
						A(4)–O(23)	3.741(12)
Cu(1)–O(25)	1.951(4)	Cu(6)–O(5)	1.970(4)	Cu(1)–O(27)	1.943(10)		
Cu(1)–O(27)	1.955(3)	Cu(6)–O(24)	1.976(4)	Cu(1)–O(25)	1.957(10)	Cu(6)–O(5)	1.964(8)
Cu(1)–O(12)	1.963(4)	Cu(6)–O(18)	1.981(4)	Cu(1)–O(12)	1.963(10)	Cu(6)–O(24)	1.971(10)
Cu(1)–O(19)	1.983(3)	Cu(6)–O(5)	1.981(4)	Cu(1)–O(19)	2.026(10)	Cu(6)–O(5)	1.984(9)
Cu(1)–O(20)	2.239(3)	Cu(6)–O(14)	2.412(4)	Cu(1)–O(20)	2.204(10)	Cu(6)–O(18)	1.986(10)
		Cu(6)–O(17)	2.477(4)			Cu(6)–O(14)	2.434(12)
						Cu(6)–O(17)	2.507(12)
Cu(2)–O(10)	1.953(4)	Cu(7)–O(8)	1.944(4)	Cu(2)–O(5)	1.961(8)		
Cu(2)–O(5)	1.958(3)	Cu(7)–O(1)	1.968(4)	Cu(2)–O(10)	1.961(10)	Cu(7)–O(8)	1.963(9)
Cu(2)–O(21)	1.962(4)	Cu(7)–O(9)	1.980(4)	Cu(2)–O(21)	1.966(10)	Cu(7)–O(9)	1.995(9)
Cu(2)–O(23)	1.967(3)	Cu(7)–O(4)	2.003(4)	Cu(2)–O(23)	2.020(10)	Cu(7)–O(4)	2.009(10)
Cu(2)–O(13)	2.231(4)	Cu(7)–O(15)	2.148(4)	Cu(2)–O(13)	2.212(11)	Cu(7)–O(1)	2.012(9)
						Cu(7)–O(15)	2.109(9)
Cu(3)–O(27)	1.895(3)	Cu(8)–O(40)	1.998(4)	Cu(3)–O(27)	1.910(8)		
Cu(3)–O(13)	1.927(4)	Cu(8)–O(35)	2.011(4)	Cu(3)–O(13)	1.949(10)	Cu(8)–O(34)	1.980(10)
Cu(3)–O(6)	2.034(4)	Cu(8)–O(34)	2.039(4)	Cu(3)–O(6)	2.024(9)	Cu(8)–O(40)	1.988(10)
Cu(3)–O(22)	2.095(4)	Cu(8)–O(36)	2.040(4)	Cu(3)–O(22)	2.093(10)	Cu(8)–O(35)	2.025(10)
Cu(3)–O(16)	2.352(4)	Cu(8)–O(30)	2.079(4)	Cu(3)–O(16)	2.448(15)	Cu(8)–O(36)	2.098(10)
Cu(3)–O(2)	2.787(4)			Cu(3)–O(2)	2.830(15)	Cu(8)–O(30)	2.107(10)
Cu(4)–O(5)	1.900(3)	Cu(9)–O(39)	1.952(4)	Cu(4)–O(5)	1.892(9)	Cu(9)–O(39)	1.977(10)
Cu(4)–O(20)	1.924(4)	Cu(9)–O(33)	1.975(4)	Cu(4)–O(20)	1.964(10)	Cu(9)–O(38)	1.997(9)
Cu(4)–O(26)	2.041(4)	Cu(9)–O(38)	1.980(4)	Cu(4)–O(26)	2.030(9)	Cu(9)–O(33)	1.999(8)
Cu(4)–O(7)	2.097(4)	Cu(9)–O(28)	1.991(4)	Cu(4)–O(7)	2.079(10)	Cu(9)–O(28)	2.000(10)
Cu(4)–O(17)	2.366(4)	Cu(9)–O(29)	2.158(4)	Cu(4)–O(17)	2.441(15)	Cu(9)–O(29)	2.109(9)
Cu(4)–O(14)	2.744(4)			Cu(4)–O(14)	2.827(15)		
Cu(5)–O(27)	1.971(4)	Cu(10)–O(31)	1.999(4)	Cu(5)–O(27)	1.973(9)	Cu(10)–O(31)	1.989(10)
Cu(5)–O(11)	1.979(4)	Cu(10)–O(37)	2.013(4)	Cu(5)–O(11)	1.976(9)	Cu(10)–O(32)	1.995(10)
Cu(5)–O(27)	1.984(4)	Cu(10)–O(32)	2.046(4)	Cu(5)–O(27)	1.982(9)	Cu(10)–O(37)	2.027(9)
Cu(5)–O(3)	1.989(4)	Cu(10)–O(41)	2.049(4)	Cu(5)–O(3)	1.987(9)	Cu(10)–O(41)	2.107(10)
Cu(5)–O(2)	2.424(4)	Cu(10)–O(42)	2.084(4)	Cu(5)–O(2)	2.422(11)	Cu(10)–O(42)	2.113(10)
Cu(5)–O(16)	2.485(4)			Cu(5)–O(16)	2.497(12)		
S(1)–O(15)	1.446(4)	S(6)–O(11)	1.464(4)	S(1)–O(15)	1.444(10)	S(6)–O(11)	1.461(9)
S(1)–O(34)	1.476(4)	S(6)–O(6)	1.467(4)	S(1)–O(36)	1.463(11)	S(6)–O(1)	1.462(9)
S(1)–O(36)	1.480(4)	S(6)–O(1)	1.471(4)	S(1)–O(34)	1.482(9)	S(6)–O(6)	1.479(9)
S(1)–O(38)	1.482(4)	S(6)–O(25)	1.475(4)	S(1)–O(38)	1.492(9)	S(6)–O(25)	1.492(11)
S(2)–O(31)	1.456(4)	S(7)–O(33)	1.466(4)	S(2)–O(39)	1.457(10)	S(7)–O(33)	1.462(9)
S(2)–O(30)	1.465(4)	S(7)–O(26)	1.468(4)	S(2)–O(31)	1.460(10)	S(7)–O(24)	1.472(10)
S(2)–O(28)	1.473(4)	S(7)–O(24)	1.470(4)	S(2)–O(30)	1.469(10)	S(7)–O(26)	1.476(10)
S(2)–O(39)	1.480(4)	S(7)–O(10)	1.471(4)	S(2)–O(28)	1.492(10)	S(7)–O(10)	1.478(9)
S(3)–O(2)	1.451(5)	S(8)–O(7)	1.469(4)	S(3)–O(2)	1.446(12)	S(8)–O(37)	1.461(10)
S(3)–O(16)	1.466(4)	S(8)–O(18)	1.470(4)	S(3)–O(16)	1.446(13)	S(8)–O(18)	1.462(10)
S(3)–O(23)	1.469(4)	S(8)–O(37)	1.475(4)	S(3)–O(23)	1.452(10)	S(8)–O(7)	1.470(10)
S(3)–O(20)	1.501(3)	S(8)–O(21)	1.476(4)	S(3)–O(20)	1.526(11)	S(8)–O(21)	1.485(11)
S(4)–O(14)	1.456(4)	S(9)–O(42)	1.461(4)	S(4)–O(17)	1.424(11)	S(9)–O(4)	1.461(10)
S(4)–O(19)	1.459(4)	S(9)–O(40)	1.462(4)	S(4)–O(14)	1.435(13)	S(9)–O(40)	1.463(11)
S(4)–O(17)	1.460(4)	S(9)–O(4)	1.473(4)	S(4)–O(19)	1.466(10)	S(9)–O(42)	1.467(9)
S(4)–O(13)	1.507(4)	S(9)–O(8)	1.475(4)	S(4)–O(13)	1.529(10)	S(9)–O(8)	1.478(9)

Table 7. (continued).

Cryptochalcite*				Cesiodymite**			
S(5)–O(3)	1.463(4)	S(10)–O(29)	1.445(4)	S(5)–O(3)	1.465(9)	S(10)–O(29)	1.448(9)
S(5)–O(22)	1.468(4)	S(10)–O(41)	1.467(4)	S(5)–O(35)	1.467(9)	S(10)–O(41)	1.455(10)
S(5)–O(35)	1.472(4)	S(10)–O(32)	1.472(4)	S(5)–O(22)	1.476(10)	S(10)–O(32)	1.472(10)
S(5)–O(12)	1.475(4)	S(10)–O(9)	1.481(4)	S(5)–O(12)	1.490(10)	S(10)–O(9)	1.482(9)

* Taking a limit of 3.50 Å for *A*–O bond.
** Taking a limit of 3.75 Å for *A*–O bond. For *A*(1) and *A*(4) additional bonds could be included: *A*(1)–O(28) = 3.758(11), *A*(1)–O(15) = 3.789 (11), *A*(4)–O(23) = 3.741(12) and *A*(4)–O(4) = 3.762(11) Å.

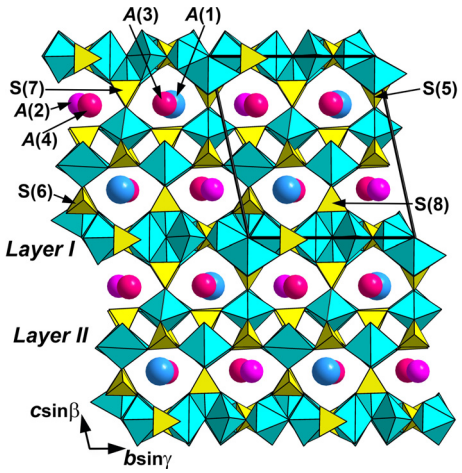

Fig. 7. The crystal structure of cryptochalcite/cesiodymite projected along the *a* axis. Cu-centred polyhedra are blue, SO_4 tetrahedra are yellow. The unit cell is outlined.

Large cations occupy four crystallographically independent *A* sites located in the tunnels of the M^{2+}-S-O heteropolyhedral framework (Fig. 7). In cesiodymite, they occupy eleven-fold [*A*(1, 2, 4)] and twelve-fold [*A*(3)] polyhedra, taking a limit of 3.75 Å for the *A*–O bond. In cryptochalcite containing much less Cs^+ than cesiodymite, the *A*(1–3) positions, mainly occupied by K^+, form eight-fold [*A*(1)] and nine-fold [*A*(2–3)] polyhedra, whereas *A*(4) is in ten-fold coordination, as in cesiodymite (taking a limit of 3.50 Å for the *A*–O bond). Occupancies for the *A* sites in both minerals (Table 6) were found on the basis of refined site-scattering values (electron counts, e_{ref}), interatomic distances (Table 7) and by taking into account electron microprobe data (Table 2). In cesiodymite admixed Rb was assumed to occupy the smallest and the lightest sites *A*(2) and *A*(4) in equal amounts, whereas most Cs is concentrated in *A*(1) (a Cs-dominant position) and *A*(3). In cryptochalcite admixed heavy alkali cations (Cs and Rb) mainly occur in the *A*(1) and *A*(3) sites characterized by the highest e_{ref} values: see footnote of Table 6. Such cation distribution is in a good agreement with the values of polyhedral volumes for *A*-centred polyhedra [calculated using Vesta 3 program (Momma & Izumi, 2011)]: for *A*(1–4) in cesiodymite they are 67.5,

57.5, 71.0 and 56.9 Å^3, respectively, and in cryptochalcite 60.5, 55.8, 60.7 and 54.5 Å^3, respectively (a limit of 3.75 Å for the *A*–O interaction was set for both structures).

The presence of Cs^+ in significant amount in cesiodymite causes its larger unit-cell dimensions and volume in comparison with cryptochalcite (Table 1).

The cryptochalcite/cesiodymite structure could also be described in terms of anion-centered tetrahedra (Krivovichev *et al.*, 2013). Two OCu_4 tetrahedra are linked *via* a common Cu–Cu edge forming $[O_2Cu_6]$ dimer (Fig. 9). The same isolated from each other $[O_2Cu_6]$ complexes were reported in euchlorine-type minerals (Scordari & Stasi, 1990; Starova *et al.*, 1991; Siidra *et al.*, 2017), in triclinic and monoclinic modifications of synthetic oxyselenite Cu $[Cu_3O](SeO_3)_3$ (Effenberger & Pertlik, 1986) and in oxyarsenate shchurovskyite, $K_2Ca[Cu_6O_2](AsO_4)_4$. Dmisokolovite, $K_3[Cu_5AlO_2](AsO_4)_4$, related to shchurovskyite, contains topologically identical dimers $[O_2Cu_5Al]$ (Pekov *et al.*, 2015a).

The structural diversity of natural H-free alkali-copper oxysulfates mentioned above, in Introduction, is shown in Fig. 10. Crystal strucutures of all these minerals are based on Cu-O-S motifs of different topology. The euchlorine structure type is characterized by the $\{Cu_3O(SO_4)_3\}^{2-}$ heteropolyhedral layers and alkali cations between them (Fig. 10a); the structurally related wulffite (Fig. 10b), parawulffite (Fig. 10c), piypite (Fig. 10g) and eleomelanite (Fig. 10d) contain $\{Cu_2O(SO_4)_2\}^{2-}$ chains of similar topology; geometrically related $\{[Cu_3O_2M(SO_4)_4\}^{3-}$ ($M = Fe^{3+}$, Al) chains are the basis of minerals of the klyuchevskite–alumoklyuchevskite isomorphous series (Fig. 10h). The kamchatkite, nabokoite and cryptochalcite structure types are based on the heteropolyhedral frameworks with quite different topologies: in kamchatkite (Fig. 10f) chains of Cu-centred polyhedra are linked by SO_4 tetrahedra forming the $Cu_3O(SO_4)_2Cl\}^-$ heteropolyhedral framework, while in nabokoite (Fig. 10i) Cu–Te–S–O–Cl layers are connected *via* Cl vertices of Cu-centred tetragonal pyramids and in cryptochalcite and cesiodymite (Fig. 10e) two types of alternating Cu-S-O polyhedral layers are connected *via* SO_4 tetrahedra to form the $\{Cu_5O(SO_4)_5\}^{2-}$ heteropolyhedral framework.

7.2. Cryptochalcite–cesiodymite solid-solution series and the K–Cs isomorphism

Cryptochalcite and cesiodymite are not only isostructural but form a solid-solution series in which the Cs:K ratio is the major variable. Composition ranges from a Cs-free cryptochalcite (Yadovitaya) to cesiodymite with Cs:K = 1.54 in a total *A* site composition $Cs_{1.03}K_{0.67}Rb_{0.21}$, with 14.7 wt% Cs_2O (#12 in Table 2). To date, a gap between samples with $(K_{1.63}Cs_{0.19}Rb_{0.15})$ and $(K_{1.18}Cs_{0.71}Rb_{0.15})$ is observed in this series (Table 2, Fig. 6).

In the holotype sample of cesiodymite with the average overall composition of the *A* sites $K_{1.14}Cs_{0.73}Rb_{0.16}$ (Table 2), dominance of Cs over K is found only in the *A*(1) site (Table 6). However, it is not the most Cs-rich specimen of the mineral. Taking into account the wide range of the Cs:K ratio in cesiodymite and possible variations of contents of these cations in different *A* sites, we consider the idealized formula $CsKCu_5O(SO_4)_5$ as the most appropriate for this mineral. This formula implies the presence of both K- and Cs-dominant *A* sites in the structure as an important crystal-chemical feature of cesiodymite. From the

formal viewpoint, the margin between the latter and cryptochalcite in this series (for the binary case) should be marked at the point with composition ($K_{1.5}Cs_{0.5}$) and between cesiodymite and a hypothetical K-free end-member $Cs_2Cu_5O(SO_4)_5$ at the point ($Cs_{1.5}K_{0.5}$). Thus, the formal compositional field of cesiodymite lies between $Cs_{0.5}K_{1.5}Cu_5O(SO_4)_5$ and $Cs_{1.5}K_{0.5}Cu_5O(SO_4)_5$. All points located on the right of the gap in Fig. 6 correspond to this formal chemical definition of cesiodymite whereas all points on the left of the gap lie in the compositional field of cryptochalcite, *i.e.*, between $Cs_{0.5}K_{1.5}Cu_5O(SO_4)_5$ and $K_2Cu_5O(SO_4)_5$.

Cesium is typical admixture constituent in some potassium minerals formed in fumaroles at the Second scoria cone of the NB GTFE. Besides cryptochalcite–cesiodymite series members, its significant amount (>1 wt % Cs_2O) was detected in wulffite (up to 1.1 wt% Cs_2O), parawulffite (up to 1.4 wt% Cs_2O) (Pekov *et al.*, 2014a), flinteite, K_2ZnCl_4 (up to 2.2 wt% Cs: Pekov *et al.*, 2015b), and averievite, $Cu_5O_2(VO_4)_2 \cdot nA$Cl, with A = K, Rb, Cs, which contains up to 4.1 wt% Cs_2O (Starova *et al.*, 1997; Vergasova *et al.*, 1998). Prior to the discovery of cesiodymite, averievite was the most Cs-rich mineral at Tolbachik. Among fumarolic minerals known from other volcanoes, avogadrite, (K,Cs)BF_4, from Vesuvius contains 7.0 wt% Cs (Anthony *et al.*, 1997).

Ordering of K and Cs is common in synthetic compounds. In minerals, almost full separation of Cs^+ and K^+ between different positions of the same crystal structure was reported in senkevichite, CsKNaTiO[Si_7O_{18}(OH)], a Cs-K-ordered analogue of tinaksite, K_2NaTiO[Si_7O_{18}(OH)] (Uvarova *et al.*, 2006), and in the zeolite-like hydrous silicates mendeleevite-(Ce) and mendeleevite-(Nd) with the general formula (Cs,□)$_6$(□,Cs)$_6$(□,K)$_6$(*REE*,Ca,□)$_{30}$($Si_{70}O_{175}$)(H_2O,OH,F,□)$_{35}$ (Sokolova *et al.*, 2011; Agakhanov *et al.*, 2017). These minerals were described from peralkaline pegmatites of the Dara-i-Pioz alkaline complex, Tadjikistan, abnormally enriched in Cs (Agakhanov *et al.*, 2005, 2017; Pautov *et al.*, 2013). For minerals of such pegmatitic systems, another type of separation of K and Cs is also common: K-depleted cesium phases occur together with Cs-depleted potassium phases, sometimes structurally related. The brightest example is an intimate association of the simultaneously crystallized isostructural micas polylithionite, $KLi_2Al(Si_4O_{10})F_2$, and sokolovaite, $CsLi_2Al(Si_4O_{10})F_2$, and the former is almost Cs-free whereas the latter is almost K-free (Pautov *et al.*, 2006). In contrast, minerals of volcanic sublimates have a disordered distribution of Cs and K. The cryptochalcite–cesiodymite series is an exception in that K and Cs are partially ordered, and the increase in Cs content of the mineral results in the appearance of Cs-dominant A sites as well as K-dominant A sites. In this way Cs is a species-defining component in cesiodymite.

Acknowledgements: This paper is dedicated to Giovanni Ferraris and Stefano Merlino for their great contributions to structural mineralogy. We thank Anthony R. Kampf and an anonymous referee for their valuable comments. This work was supported by the Russian Science Foundation, grant no. 14-17-00048. The technical support by the SPbSU X-Ray Diffraction Resource Center in the powder XRD study of cesiodymite is acknowledged.

References

Agakhanov, A.A., Pautov, L.A., Uvarova, Y.A., Sokolova, E.V., Hawthorne, F.C., Karpenko, V.Yu. (2005): Senkevichite CsKNaCa$_2$TiO[Si_7O_{18}(OH)], a new mineral. *New Data Miner.*, **40**, 17–22.

Agakhanov, A.A., Pautov, L.A., Sokolova, E., Hawthorne, F.C., Karpenko, V.Yu., Siidra, O.I., Garanin, V.K. (2017): Mendeleevite-(Nd), (Cs,□)$_6$(□,Cs)$_6$(□,K)$_6$(*REE*,Ca)$_{30}$($Si_{70}O_{175}$)(OH,H_2O,F)$_{35}$, a new mineral from the Darai-Pioz alkaline massif, Tajikistan. *Mineral. Mag.*, **81**, 135–141.

Agilent Technologies (2014): CrysAlisPro Software system, version 1.171.37.35. Agilent Technologies UK Ltd, Oxford, UK.

Anthony, J.W., Bideaux, R.A., Bladh, K.W., Nichols, M.C. (1997): Handbook of Mineralogy, III. Halides, Hydroxides, Oxides. Mineral Data Publishing, Tucson.

Brese, N.E. & O'Keeffe, M. (1991): Bond-valence parameters for solids. *Acta Crystallogr. B*, **47**, 192–197.

Burns, P.C. & Hawthorne, F.C. (1995): Mixed-ligand $Cu^{2+}\Phi_6$ octahedra in minerals: observed stereochemistry and Hartree-Fock calculations. *Can. Mineral.*, **33**, 1177–1188.

Clark, R.C. & Reid, J.S. (1995): The analytical calculation of absorption in multifaceted crystals. *Acta Crystallogr. A*, **51**, 887–897.

Effenberger, H. & Pertlik, F. (1986): Die Kristallstrukturen der Kupfer(II)-oxo-selenite $Cu_2O(SeO_3)$ (kubisch und monoklin) und $Cu_4O(SeO_3)_3$ (monoklin und triklin). *Monatshefte für Chem.*, **117**, 887–896.

Effenberger, H. & Zemann, J. (1984): The crystal structure of caratiite. *Mineral. Mag.*, **48**, 541–546.

Fedotov, S.A. & Markhinin, Y.K., (1983): The Great Tolbachik Fissure Eruption. Cambridge Univ. Press, New York.

Gorskaya, M.G., Filatov, S.K., Rozhdestvenskaya, I.V., Vergasova, L.P. (1992): The crystal structure of klyuchevskite, K_3Cu_3(Fe,Al)$O_2(SO_4)_4$, a new mineral from Kamchatka volcanic sublimates. *Mineral. Mag.*, **56**, 411–416.

Gorskaya, M.G., Vergasova, L.P., Filatov, S.K., Rolich, D.V., Ananiev, V.V. (1995): Alumoklyuchevskite, $K_3Cu_3AlO_2(SO_4)_4$, a new oxysulfate of K, Cu and Al from volcanic exhalations, Kamchatka, Russia. *Zapiski VMO*, **124**, 95–100 (in Russian).

Krivovichev, S.V., Filatov, S.K., Cherepansky, P.N. (2009): The crystal structure of alumoklyuchevskite, $K_3Cu_3AlO_2(SO_4)_4$. *Geol. Ore Depos.*, **51**, 656–662.

Krivovichev, S.V., Mentre, O., Siidra, O.I., Colmont, M., Filatov, S. K. (2013): Anion-centered tetrahedra in inorganic compounds. *Chem. Rev.*, **113**, 6459–6535.

Momma, K. & Izumi, F. (2011): VESTA 3 for three-dimensional visualization of crystal, volumetric and morphology data. *J. Appl. Crystallogr.*, **44**, 1272–1276.

Nakamoto, K. (1986): Infrared and Raman Spectra of Inorganic and Coordination Compounds. John Wiley & Sons, New York.

Pautov, L.A., Agakhanov, A.A., Bekenova, G.K. (2006): Sokolovaite $CsLi_2AlSi_4O_{10}F$ – a new mineral species of the mica group. *New Data on Miner.*, **41**, 5–13.

Pautov, L.A., Agakhanov, A.A., Karpenko, V.Yu., Sokolova, E.V., Hawthorne, F.C. (2013): Mendeleevite-(Ce), (Cs,□)$_6$(□,Cs)$_6$(□,K)$_6$(*REE*,Ca,□)$_{30}$($Si_{70}O_{175}$)(H_2O,OH,F,□)$_{35}$, a new mineral from the Darai-Pioz massif, Tajikistan. *Dokl. Earth Sci.*, **552**, 1023–1026.

Pekov, I.V., Zubkova, N.V., Yapaskurt, V.O., Belakovskiy, D.I., Chukanov, N.V., Lykova, I.S., Saveliev, D.P., Sidorov, E.G., Pushcharovsky, D.Yu. (2014a): Wulffite, $K_3NaCu_4O_2(SO_4)_4$, and parawulffite, $K_5Na_3Cu_8O_4(SO_4)_8$, two new minerals from fumarole sublimates of the Tolbachik volcano, Kamchatka, Russia. *Can. Mineral.*, **52**, 699–716.

Pekov, I.V., Zubkova, N.V., Yapaskurt, V.O., Belakovskiy, D.I., Lykova, I.S., Vigasina, M.F., Sidorov, E.G., Pushcharovsky, D. Yu. (2014b): New arsenate minerals from the Arsenatnaya fumarole, Tolbachik volcano, Kamchatka, Russia. I. Yurmarinite, $Na_7(Fe^{3+}, Mg, Cu)_4(AsO_4)_6$. *Mineral. Mag.*, **78**, 905–917.

Pekov, I.V., Zubkova, N.V., Belakovskiy, D.I., Yapaskurt, V.O., Vigasina, M.F., Sidorov, E.G., Pushcharovsky D.Y. (2015a): New arsenate minerals from the Arsenatnaya fumarole, Tolbachik volcano, Kamchatka, Russia. IV. Shchurovskyite, $K_2CaCu_6O_2(AsO_4)_4$, and dmisokolovite, $K_3Cu_5AlO_2(AsO_4)_4$. *Mineral. Mag.*, **79**, 1737–1753.

Pekov, I.V., Zubkova, N.V., Yapaskurt, V.O., Britvin, S.N., Vigasina, M.F., Sidorov, E.G., Pushcharovsky, D.Yu. (2015b): New zinc and potassium chlorides from fumaroles of the Tolbachik volcano, Kamchatka, Russia: mineral data and crystal chemistry. II. Flinteite, K_2ZnCl_4. *Eur. J. Mineral.*, **27**, 581–588.

Pekov, I.V., Zubkova, N.V., Agakhanov, A.A., Chukanov, N.V., Belakovskiy, D.I., Sidorov, E.G., Britvin, S.N., Pushcharovsky, D.Y. (2016): Eleomelanite, IMA 2015-118. CNMNC Newsletter No. 30, April 2016, page 412. *Mineral. Mag.*, **80**, 407–413.

Pekov, I.V., Koshlyakova, N.N., Zubkova, N.V., Lykova, I.S., Britvin, S.N., Yapaskurt, V.O., Agakhanov, A.A., Shchipalkina, N.V., Turchkova, A.G., Sidorov, E.G. (2018): Fumarolic arsenates – a special type of arsenic mineralization. *Eur. J. Mineral.*, **30**, in press.

Pertlik, F. & Zemann, J. (1988): The crystal structure of nabokoite, $Cu_7TeO_4(SO_4)_5 \cdot KCl$: the first example of a $Te(IV)O_4$ pyramid with exactly tetragonal symmetry. *Mineral. Petrol.*, **38**, 291–298.

Popova, V.I., Popov, V.A., Rudashevskiy, N.S., Glavatskikh, S.F., Polyakov, V.O., Bushmakin, A.F. (1987): Nabokoite $Cu_7TeO_4(SO_4)_5 \cdot KCl$ and atlasovite $Cu_6Fe^{3+}Bi^{3+}O_4(SO_4)_5 \cdot KCl$. New minerals of volcanic exhalations. *Zapiski VMO*, **116**, 358–367 (in Russian).

Scordari, F. & Stasi, F. (1990): The crystal structure of euchlorin, $NaKCu_3O(SO_4)_3$. *N. Jahrb. Mineral. Monatsh.*, 241–253.

Sheldrick, G.M. (2015): Crystal structure refinement with SHELXL. *Acta Crystallogr. C*, **71**, 3–8.

Siidra, O.I., Nazarchuk, E.V., Zaitsev, A.N., Lukina, E.A., Avdontseva, E.Y., Vergasova, L.P., Vlasenko, N.S., Filatov, S. K., Turner, R., Karpov, G.A. (2017): Copper oxosulphates from fumaroles of Tolbachik volcano: puninite, $Na_2Cu_3O(SO_4)_3$-a new mineral species and structure refinements of kamchatkite and alumoklyuchevskite. *Eur. J. Mineral*., **29**, 499–510.

Sokolova, E., Hawthorne, F.C., Pautov, L.A., Agakhanov, A.A., Karpenko, V.Yu. (2011): The crystal structure and crystal chemistry of mendeleevite-(Ce), $(Cs,\square)_6(\square,Cs)_6(\square,K)_6(REE, Ca,\square)_{30}(Si_{70}O_{175})(H_2O,OH,F,\square)_{35}$, a potential microporous material. *Mineral. Mag.*, **75**, 2583–2596.

Starova, G.L., Filatov, S.K., Fundamensky, V.S., Vergasova, L.P. (1991): The crystal structure of fedotovite, $K_2Cu_3O(SO_4)_3$. *Mineral. Mag.*, **55**, 613–616.

Starova, G.L., Krivovichev, S.V., Fundamenskii, V.S., Filatov, S.K. (1997): The crystal structure of averievite, $Cu_5O_2(VO_4)_2 \cdot nMX$: comparison with related compounds. *Mineral. Mag.*, **61**, 441–446.

Uvarova, Y.A., Sokolova, E., Hawthorne, F.C., Agakhanov, A.A., Pautov, L.A., Karpenko, V.Yu. (2006): The crystal chemistry of senkevichite, $CsKNaTiO[Si_7O_{18}(OH)]$, from the Dara-i-Pioz alkaline massif, Northern Tajikistan. *Can. Mineral.*, **44**, 1341–1349.

Varaksina, T.V., Fundamensky, V.S., Filatov, S.K.,Vergasova, L.P. (1990): The crystal structure of kamchatkite, a new naturally occurring oxychloride sulphate of potassium and copper. *Mineral. Mag*., **54**, 613–616.

Vergasova, L.P. & Filatov, S.K. (2016): A study of volcanogenic exhalation mineralization. *J. Volcanol. Seismol.*, **10**, 71–85.

Vergasova, L.P., Filatov, S.K., Serafimova, E.K., Starova, G.L. (1984): Piypite, $K_2Cu_2O(SO_4)_2$, a new mineral of volcanic exhalations. *Dokl. AN SSSR*, **275**, 714–717 (in Russian).

—, —, —, — (1988a): Fedotovite, $K_2Cu_3O(SO_4)_3$, a new mineral of volcanic exhalations. *Dokl. AN SSSR*, **299**, 961–964 (in Russian).

Vergasova, L.P., Filatov, S.K., Serafimova, E.K., Varaksina, T.V. (1988b): Kamchatkite, $KCu_3OCl(SO_4)_2$, a new mineral of volcanic sublimates. *Zapiski VMO*, **117**, 459–461 (in Russian).

Vergasova, L.P., Filatov, S.K., Gorskaya, M.G., Ananiev, V.V., Sharov, A.S. (1989): Klyuchevskite, $K_3Cu_3(Fe, Al)O_2(SO_4)_4$, a new mineral from volcanic exhalations. *Zapiski VMO*, **118**, 70–73 (in Russian).

Vergasova, L.P., Starova, G.L., Filatov, S.K., Ananiev, V.V. (1998): Averievite $Cu_5O_2(VO_4)_2 \cdot nMX$ – a new mineral of volcanic exhalations. *Dokl. Ross. Akad. Nauk*, **359**, 804–807 (in Russian).

Received 28 June 2017
Modified version received 14 October 2017
Accepted 14 October 2017